# Young's Double-Slit Interference in a Hydrogen Atom

Pei-Lun He,[1,*] Zhao-Han Zhang,[1] and Feng He[1,2,†]
[1]Key Laboratory for Laser Plasmas (Ministry of Education) and School of Physics and Astronomy, Collaborative Innovation Center for IFSA (CICIFSA), Shanghai Jiao Tong University, Shanghai 200240, China
[2]CAS Center for Excellence in Ultra-intense Laser Science, Shanghai, 201800, China

(Received 30 September 2019; revised manuscript received 20 February 2020; accepted 7 April 2020; published 21 April 2020)

We demonstrate the possibility of realizing Young's double-slit interference in a hydrogen atom via *ab initio* simulations. By exposing the hydrogen atom to a high-frequency intensive laser pulse, the bound state distorts into a dichotomic Kramers-Henneberger state whose photoelectron momentum distribution imprints a double-slit interference structure. The dichotomic hydrogen atom presents molecular peculiarities, such as charge-resonance enhanced ionization, electron spin flipping due to the non-Abelian Berry phase. In return, the photoelectron momentum distribution carrying the double-slit interference structure provides unambiguous evidence on the existence of Kramers-Henneberger states, and thus the adiabatic stabilization.

DOI: 10.1103/PhysRevLett.124.163201

Double-slit interference, with which Young explicated light as waves in 1801, is one of the most vital experiments in history. Though more than two hundred years had passed, double-slit experiments continue to provide insights into both fundamental research and practical applications nowadays. For example, which-way information experiments provide testimony to the basic principle of quantum mechanics [1–3], a matterless double-slit experiment explored the fluctuation of vacuum [4], and the interference in the electron pair demonstrates the universal nonlocality of quantum entanglement [5]. As practical applications, double-slit interference can measure light coherence [6], detect molecular structures [7], and retrieve the motion of nuclei [8].

The double-slit experiment can be performed in diatomic molecules, in which the two Coulomb centers work as the double slits, and the valence electron plays the role of light in the original Young's experiment. The theoretical prediction made by Cohen and Fano [9] had been observed in molecules such as $H_2$ [10,11], $N_2$ [12], neon dimmer [13], etc. It sounds counterintuitive to have such kind of double-slit interference in an atom since one atom is impossible to offer two Coulomb centers. However, there existed nontrivial analogies in the time domain. Lindner *et al.* [14] designed such kind of double slits, in which the ionization bursts produced by two successive wave crests of a few-cycle phase-stabilized pulse interfere with each other. These time-domain double slits were further studied by adding another orthogonally polarized streaking pulse [15,16]. Recently, Pursehouse *et al.* [17] considered a two-path ionization of a rubidium atom via intermediate $5P$ and $6P$ states, in which the excitation path is undetermined and the interference in wave-vector space is analogous to double-slit interference.

The existence of metastable Kramers-Henneberger states (KHSs) [18–20], which are the eigenstates of the time-averaged Hamiltonian in a high-frequency laser field [21], provides a possibility of realizing the double-slit interference in an atom. The KHS is known to be relevant for ionization stabilization [22], low-energy photoelectron generated by the nonadiabatic coupling [23,24], and dynamic interference [25–27]. The KHS plays an important role as long as the systems have exact or approximate Floquet symmetry [28]. However, while the acceleration of neutral atoms [29,30] and the amplifying of air lasing [31,32] provide tantalizing hints [20], there is still no "smoking gun" evidence for a direct experimental confirmation of the KHS up to now. The ionization stabilization of Rydberg atoms [33] does not provide convincible evidence since the nonadiabatic coupling [23,24] in intensive fields always populates a superposition of Rydberg states, as their energy gaps are small, interference stabilization [34] might be responsible for the observed phenomena. The unavoidable focal intensity volume average effect in practice implies that the ionization signals are always from a mixture of KHSs and laser-free bound states. Thus, shifts of the photoelectron kinetic energy [35] and fine structures of the photoelectron momentum distribution (PMD) from the KH atom [36] are blurred after the focal intensity volume average.

In this Letter, we demonstrate the possibility of realizing molecular Young's double-slit interference using a single hydrogen atom. By exposing the atom to a high-frequency intensive laser field, the distorted bound state forms a dichotomic KHS [37,38]. When the atom gets ionized by a probe pulse, the PMD carries its structural information. The distinct angularly distributed PMD is robust against the focal intensity volume average, which provides

 

unambiguous evidence on the existence of KHSs in intense laser fields, and thus adiabatic stabilization. The adiabatically rotating double slits could induce spin flipping, which is a manifestation of the Berry phase.

We perform *ab initio* simulations and start with the three-dimensional time-dependent Schrödinger equation (TDSE) in the Kramers-Henneberger (KH) frame [21] (atomic units are used throughout unless stated otherwise):

$$i\frac{\partial}{\partial t}\psi(\mathbf{r},t)=\left[\frac{\mathbf{p}^2}{2}+V_C(\mathbf{r}+\boldsymbol{\beta}_1(t))+\mathbf{p}\cdot\mathbf{A}_2(t)\right]\psi(\mathbf{r},t), \quad (1)$$

where $V_C(\mathbf{r})=-1/|\mathbf{r}|$ is the Coulomb potential. The laser field is described as

$$\mathbf{E}_i(t)=\beta_i\omega_i^2[\cos(\omega_i t+\varphi_i)\mathbf{e}_x-\varepsilon_i\sin(\omega_i t+\varphi_i)\mathbf{e}_y]\times\cos^2\left(\pi\frac{t}{L_i}\right), \quad -L_i/2<t<L_i/2, \quad (2)$$

where $i=1, 2$ stands for the pump pulse and probe pulse, respectively, $\varphi_i$ is the carrier envelope phase (CEP), $\varepsilon_i$ is the ellipticity, $L_i$ is the pulse duration, $\mathbf{A}_i(t)=-\int^t dt\mathbf{E}_i$ is the vector potential, and $\boldsymbol{\beta}_i(t)=\int^t dt\mathbf{A}_i$ is the time-dependent displacement. For all parameters considered in this Letter, $\mathbf{A}_i$ vanishes when the laser is turned off. The delay between the pump and the probe pulse is zero. We have tested that our conclusions are not blurred by the nondipole effect and the shape of the pulse envelope. The ground state of Eq. (1) is obtained using the imaginary time method, and the split-operator method is applied to propagate the wave function in real time [39]. We propagate the wave packet after the end of the laser pulse and obtain the PMD by Fourier transforming the wave function when the ionized parts propagate to the area $|\mathbf{r}|>50$ a.u. The convergence has been checked by comparing it with the PMDs obtained by projecting to the scattering states.

Dynamics of laser-matter interactions in the high-frequency regime could be conveniently described by expanding the laser-distorted Coulomb potential as $V_C[\mathbf{r}+\boldsymbol{\beta}_1(t)]\approx\sum_N V_N(\mathbf{r};t)e^{-iN\omega_1 t}$ [21], where $V_N(\mathbf{r};t)=\int_{-T_1/2}^{T_1/2}d\tau V_C[\mathbf{r}+\boldsymbol{\beta}_1(t+\tau)]\exp(iN\omega_1\tau)/T_1$ and $T_1=2\pi/\omega_1$ is the laser optical period. $V_0$ is a laser-dressed adiabatic potential, while the nonzero harmonic components $V_N$ induce photon absorption or emission. It was known that $V_0$ has a dichotomic structure when $\mathbf{A}_1$ is linearly polarized [37,38]. As a consequence, the distorted bound-state electron wave packet, i.e., the KHS, also presents a dichotomic structure. The existence of the KHS can be affirmed by the photoelectron released by the probe pulse. The probe pulse should be intense enough to trigger noticeable ionization but not too strong that the formed double slits get destroyed, which thereby imposes a condition $\beta_2\ll\beta_1$.

We present the PMD in Fig. 1. The pump pulse is linearly polarized along the $x$ axis ($\varepsilon_1=0$) with a duration of $L_1=20T_1$, and the probe pulse is circularly polarized in the $x$-$y$ plane ($\varepsilon_2=1$) with a duration of $L_2=20T_2$. The upper row of Fig. 1 shows the above-threshold ionization (ATI) released by absorbing photons of the bichromatic pulse. The left and right columns are for the cases when the hydrogen atom is initially in the $1s$ and $2p_x$ states, respectively. Though the probability of absorbing the probe-pulse photons is small due to its relatively weak intensity, ionization induced by the probe pulse contributes photoelectron with distinguished angular distribution and non-overlapping energy, compared with the ionization fragments induced by the pump pulse. Thus one can easily separate one-probe-photon ionization from the dominating pump-photon ionization. A higher frequency $\omega_1$ is not only more convenient for separating the ionization events generated by the pump and the probe pulses [40] but also better for avoiding ionization depletion [42], though the required laser intensity is much higher. The KH potential

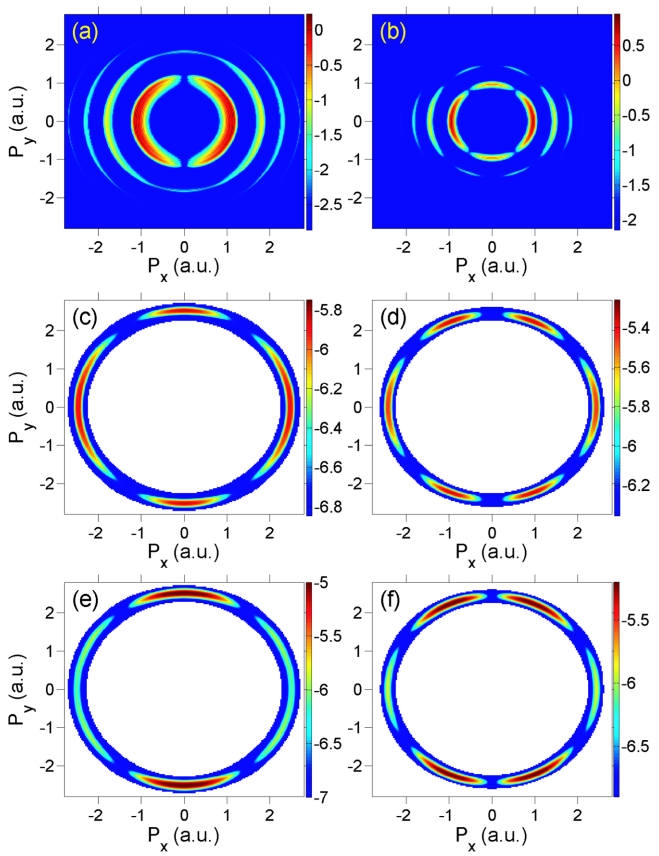


FIG. 1. PMDs contributed by the bichromatic pulse (top row), signals of one-probe-photon ionization (middle row), and signals of one-probe-photon ionization obtained via perturbative Eq. (3) (bottom row). (Left column) The hydrogen atom is initially in the $1s$ state, the laser parameters are $\omega_1=1, \beta_1=2$ ($I_1=1.4\times10^{17}$ W/cm$^2$), and $\omega_2=3.5$ a.u. (Right column) The hydrogen atom is initially in the $2p_x$ state, the laser parameters are $\omega_1=0.6125$, $\beta_1=2$ ($I_1=2.2\times10^{16}$ W/cm$^2$), and $\omega_2=3.125$ a.u. The probe pulse has an intensity of $I_2=1\times10^{15}$ W/cm$^2$.

$V_0$ is axially symmetric in the $x$-$y$ plane [43], thus, the $1s$ hydrogen atom is distorted to a $1s\sigma_g$ state by the pump pulse. As the parity is even, the PMD has a local maximum at $P_x = 0$, as shown in Fig. 1(c). Similarly, the $2p_x$ hydrogen atom is distorted to a $2p\sigma_u$ state with the odd parity, and the corresponding PMD has a local minimum at $P_x = 0$ a.u., as shown in Fig. 1(d). In practice, the $2p_x$ hydrogen atom can be prepared via a resonant excitation from the $1s$ state by a linearly polarized pulse.

To prove the PMD in Figs. 1(c) and 1(d) is indeed ionized from the KHS formed by the pump pulse, we calculate the transition amplitude using the perturbation theory

$$M(\mathbf{p}) = -i \int dt \int d\mathbf{r} e^{i[\mathbf{p}^2/2 - E_{\mathrm{KH}}(\beta_1)]t} \times e^{-i\mathbf{p}\cdot\mathbf{r}} \mathbf{p} \cdot \mathbf{A}_2(t) \psi_{\mathrm{KH}}(\mathbf{r};\beta_1), \quad (3)$$

where $\psi_{\mathrm{KH}}(\mathbf{r};\beta_1)$ is the eigenstate of the KH Hamiltonian

$$\left(\frac{\mathbf{p}^2}{2} + \tilde{V}_0(\mathbf{r};\beta_1)\right)\psi_{\mathrm{KH}}(\mathbf{r};\beta_1) = E_{\mathrm{KH}}(\beta_1)\psi_{\mathrm{KH}}(\mathbf{r};\beta_1). \quad (4)$$

The KH potential $\tilde{V}_0(\mathbf{r};\beta_1)$ is defined via $\tilde{V}_0(\mathbf{r};\beta_1) = (1/2\pi)\int_{-\pi}^{\pi} d\phi V_C(\mathbf{r} + \beta_1 \sin\phi \mathbf{e}_x)$. The perturbative results presented in the bottom row of Fig. 1 capture the essential features of TDSE simulations. Positions of local minima and the photoelectron kinetic energy $E_{\mathbf{k}} = \omega_2 + E_{\mathrm{KH}}(\beta_1)$ [35] are reproduced by Eq. (3). We note the positions of local minima depend only on $\beta_1$ and are located at $P_x \approx n\pi/\beta_1$, here $n$ is an integer, which is further checked with a wide variety of parameters in the Supplemental Material [40]. The PMDs in Figs. 1(c) and 1(e) present the structure that is more similar to Fraunhofer diffraction, whereas clear double-slit interference structures are shown in Figs. 1(d) and 1(f). To see distinct double-slit interference for a $1s$ atom, a multicolor pump pulse is suggested [40].

To judge the experimental feasibility of the above pump-probe scheme, we must take into account the unavoidable focal-intensity volume average effect. By assuming that the intensity of the laser pulse has a Gaussian spatial distribution [44], we plot the focal-intensity-averaged photoelectron angular distribution in Fig. 2, in which the top and bottom rows are the results when the initial states are $1s$ and $2p_x$, and the three columns are the results using different laser intensities (parameters shown in the caption). Distinctive angle-dependent ionization yields induced by the probe pulse are presented, and we thus conclude that the angular distribution in Fig. 1 is robust against the intensity average effect. As the number of nodes is determined by $\beta_1\sqrt{2E_{\mathbf{k}}}$, a larger probe pulse frequency has the advantage to produce distinct angular lobes [40].

The scenario is different when the probe pulse induces tunneling ionization as shown in Fig. 3. Here the pump

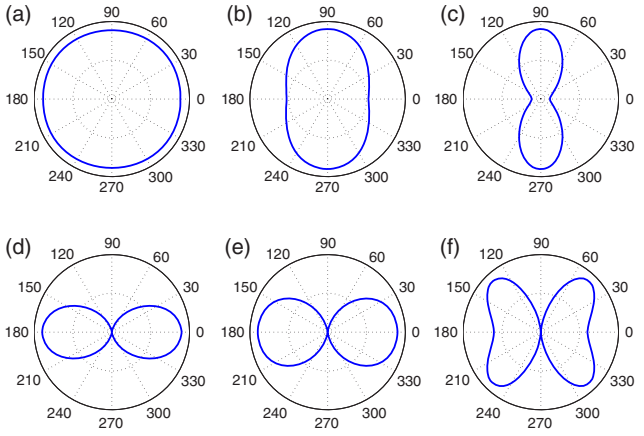


FIG. 2. Focal-intensity averaged photoelectron angular distributions. (Top row) The atom is initially in the $1s$ state, and the intensity of the pump pulse is (a) $I_1 = 0 \times 10^{16}$ ($\beta_1 = 0$ a.u.), (b) $I_1 = 3.5 \times 10^{16}$ ($\beta_1 = 1$ a.u.), and (c) $I_1 = 1.4 \times 10^{17}$ W/cm$^2$ ($\beta_1 = 2$ a.u.). Other parameters are the same as Fig. 1(c). (Bottom row) The atom is initially in the $2p_x$ state, and the intensity of the pump pulse is (d) $I_1 = 0 \times 10^{16}$ ($\beta_1 = 0$ a.u.), (e) $I_1 = 0.51 \times 10^{16}$ ($\beta_1 = 1$ a.u.), and (f) $I_1 = 2.0 \times 10^{16}$ W/cm$^2$ ($\beta_1 = 2$ a.u.). Other parameters are the same as Fig. 1(d).

pulse is a thirty-cycle 30 nm pulse with $\beta_1 = 1$ a.u. ($I_1 = 8.1 \times 10^{16}$ W/cm$^2$), and the probe pulse is a four-cycle 800 nm pulse with an intensity of $I_2 = 6 \times 10^{13}$ W/cm$^2$. The duration of the pump pulse is much shorter than the duration of the probe pulse, and the KHS experiences different electric fields if the circularly polarized probe pulse has a different CEP. As shown in Figs. 3(a) and 3(b), the photoelectrons are streaked to different directions. The laser dressed KH potential $\tilde{V}_0(\mathbf{r};\beta_1)$ is dichotomic, thus the KHS has a similar structure as $H_2^+$ [45] and is preferentially ionized when the laser field is parallel to the elongated wave packet. As a consequence, the CEP-averaged PMD presented in Fig. 3(c) has an anisotropic distribution. The local maximum deviates from the $y$ axis, which is a consequence of electron streaking in the presence of the Coulomb field. Similar to the case of $H_2^+$, such a deviation is a function of $\beta_1$ and $I_2$ [46]. For reference, we turn off the pump pulse, and the PMD induced by the circularly polarized probe pulse presents concentric circles, as shown in Fig. 3(d).

Comparing Fig. 1 with Fig. 3, the behaviors of the KHS in XUV and IR probe pulses are quite different. While the formation of the KHS reduces the ionization probability in high-frequency laser fields [22], it gives rise to significant ionization enhancement in low-frequency laser fields. In Figs. 4(a) and 4(b), we plot the $\beta_1$-dependent ionization yields when the ground KHS of the hydrogen atom exposed to high- and low-frequency laser fields, respectively. In these calculations, a preprepared $|\psi_{\mathrm{KH}}(\beta_1)\rangle$ is adopted as the initial state for the following TDSE simulation

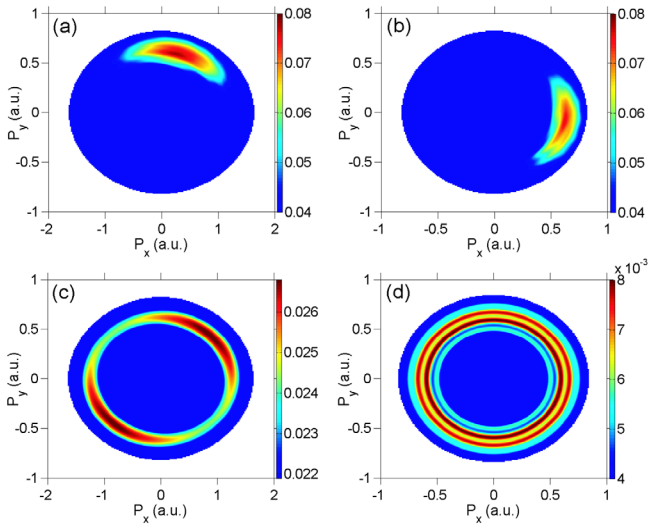


FIG. 3. PMDs contributed by an IR probe pulse. The pump laser is a thirty-cycles 30 nm pulse. We have (a)–(c) $\beta_1 = 1$ a.u. and (d) $\beta_1 = 0$ a.u. The probe pulse is a four-cycles 800 nm pulse with an intensity of $I_2 = 6 \times 10^{13}$ W/cm$^2$. The CEP of the probe pulse is (a) $\varphi_2 = 0$, (b) $\varphi_2 = \pi/4$. We present the CEP averaged PMDs in (c) and (d). The delay between the pump and probe pulses is zero.

$$i\frac{\partial}{\partial t}|\psi_{\mathrm{KH}}(t;\beta_1)\rangle = \left[\frac{1}{2}\mathbf{p}^2 + \tilde{V}_0(\beta_1) + \mathbf{p}\cdot\mathbf{A}_2(t)\right]|\psi_{\mathrm{KH}}(t;\beta_1)\rangle. \tag{5}$$

In Fig. 4(a), the KH hydrogen atom is ionized by an XUV pulse with an intensity of $10^{15}$ W/cm$^2$. The distortion of the wave function reduces the photon absorption cross section [22], which suppresses the ionization yields with an increase of $\beta_1$ as a manifestation of stabilization. In Fig. 4(b), the ground-state KH hydrogen is ionized by an IR pulse with a wavelength of 800 (red), 1200 (blue), and 1600 nm (black). The peaks of the three curves locate at $\beta_1 = 3.5$, 5.0, and 6.5 a.u.. At these $\beta_1$, the photon energy $\omega_2$ is resonant to the energy difference of the two lowest KHSs [43], which is the token of the charge resonance enhanced ionization in diatomic molecules [47,48]. The several orders of magnitude difference between Figs. 4(a) and 4(b) explains the dramatically different ionization probabilities between Fig. 1 and Fig. 3.

The axially symmetric dichotomic KH potential $\tilde{V}_0(\mathbf{r};\beta_1)$ implies states with degenerate energies, e.g., spin-up and spin-down states related by the time-reversal symmetry, would be mixed due to the non-Abelian geometric phase [49–51] when the laser polarization axis rotates adiabatically. The effect under consideration originates from the KH potential and the resulting spin-orbital coupling. The oscillating harmonic components are irrelevant for the spin dynamics as we are only concerned about the survival neutral atom and the harmonic components contribute to ionization. The theoretical formalism is parallel to the case of diatomic molecules [49], and we present details of derivation in the Supplemental Material [40]. Consider the situation that the laser field is initially linearly polarized along the $z$ axis. One adiabatically rotates the polarization axis by $\theta_0 = \pi/2$ in the $z$-$x$ plane, then rotates it by $\phi_0$ in the $x$-$y$ plane, and finally rotates it back to the $z$ axis. The rotation of the polarization axis could be realized via a sequence of polarization-skewed pulses [52]. Because of the spin-orbital coupling, the $2p\pi_u$ states split into states of $M = \pm\frac{1}{2}$ and $M = \pm\frac{3}{2}$, which we label as $|\psi_2, M = \pm\frac{1}{2}\rangle$ and $|\psi_2, M = \pm\frac{3}{2}\rangle$. Here $M$ is the projection of total angular momentum $\mathbf{J}$ along the laser polarization axis. The criteria for the adiabatic rotation can be satisfied when the duration of the rotating pulse is much longer than picoseconds [40], with which the fine energy splitting between $|\psi_2, M = \pm\frac{1}{2}\rangle$ and $|\psi_2, M = \pm\frac{3}{2}\rangle$ can be resolved. The spin-flipping probability between $|\psi_2, M = \frac{1}{2}\rangle$ and $|\psi_2, M = -\frac{1}{2}\rangle$ is $\cos^2(\kappa\pi/2)\sin^2(\kappa\phi_0/2)$, where $\kappa = 2\langle\psi_2, M = \frac{1}{2}|J_x|\psi_2, M = -\frac{1}{2}\rangle$ is of the order $O(1/c^2)$ and $c$ is the light speed. Taking $\phi_0 = \pi/\kappa$, a nearly complete spin flipping could be achieved. For the $1s\sigma_g$ and $2p\sigma_u$ states, we have $\kappa \approx 1$, and the spin flipping is nearly forbidden. For $|\psi_2, M = \pm\frac{3}{2}\rangle$ state, the geometric phase is Abelian and no spin flipping could happen [49]. Though the spin-polarized photoelectrons have been exclusively generated by the selective ionization [53–57], there is little dynamical spin flipping due to the weakness of spin-magnetic coupling [58]. The formation of the spatial double slits in atoms provides a new route to control spin dynamics with intense laser fields. Consider an ensemble of unpolarized ground-state hydrogen atoms irradiated by a resonantly left-hand circularly polarized pulse, we obtain an ensemble with the states $|\psi_2, M = \frac{3}{2}\rangle$ and $|\psi_2, M = \frac{1}{2}\rangle$. Putting these states into the properly adiabatically rotating laser field, we end up with an ensemble of hydrogen atoms with spin-up. Before ending this topic, we may point that a femtosecond rotating pulse will give a different conclusion

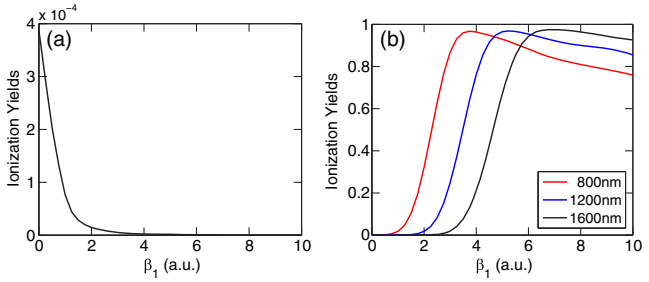


FIG. 4. Ionization yields as a function of $\beta_1$ when the ground-state KH hydrogen is (a) single-photon ionized by a 13 nm XUV pulse and (b) tunneling ionized by a four-cycle IR pulse. The XUV pulse has a duration of $L_2 = 20T_2$ and an intensity of $I_2 = 1 \times 10^{15}$ W/cm$^2$. The wavelength of the IR pulse is 800 (red), 1200 (blue), and 1600 nm (black). The intensity of the IR pulse is tuned so that $\beta_2\omega_2$ is in agreement with Fig. 3.

because it cannot resolve the fine energy splitting between $|\psi_2, M = \pm\frac{1}{2}\rangle$ and $|\psi_2, M = \pm\frac{3}{2}\rangle$. In this case, one should treat these states as fourfold degeneracy, which results in magnetic moment flipping with a probability of $\sin^2(\kappa\phi_0\pi/4)$ instead of spin flipping [40]. The currently available laser parameters in experiments are far from a perfect implementation of the spin control via the rotating polarization axis, however, the considered magnetic moment flipping process might be accessible.

In summary, the high-frequency intensive laser field can severely distort the bound state of the hydrogen atom to form a KHS with a double-slit structure. The electron may be emitted from either slit and produce the double-slit interference in the photoelectron momentum distribution, which is not only of conceptual importance but also provides unambiguous evidence on the existence of Kramers-Henneberger states, and thus adiabatic stabilization. Because of the formation of the double slits, scenarios occurred in diatomic molecules such as charge-resonance enhanced ionization and electron spin flipping due to the non-Abelian Berry phase are observed in atoms for the first time. An experimental realization of Young's double-slit interference in a hydrogen atom requires a laser intensity of $I_1 = 10^{15}$–$10^{17}$ W/cm$^2$ when the laser wavelength is dozens of nanometers [40], which is within the reach of current laser facilities [59]. Our study deepens the understanding of matter's property in high-frequency strong laser fields and opens the door to study molecular physics using isolated atoms.

This work was supported by National Key R&D Program of China (2018YFA0404802), Innovation Program of Shanghai Municipal Education Commission (2017-01-07-00-02-E00034), National Natural Science Foundation of China (NSFC) (Grants No. 11925405, No. 11721091, No. 91850203), and Shanghai Shuguang Project (17SG10). Simulations were performed on the $\pi$ supercomputer at Shanghai Jiao Tong University.

*a225633@sjtu.edu.cn
†fhe@sjtu.edu.cn

[1] X. J. Liu, Q. Miao, F. Gel'Mukhanov, M. Patanen, O. Travnikova, C. Nicolas, H. Å. gren, K. Ueda, and C. Miron, Einstein-Bohr recoiling double-slit gedanken experiment performed at the molecular level, Nat. Photonics **9**, 120 (2015).
[2] A. G. Manning, R. I. Khakimov, R. G. Dall, and A. G. Truscott, Wheeler's delayed-choice gedanken experiment with a single atom, Nat. Phys. **11**, 539 (2015).
[3] Y. Xiao, H. M. Wiseman, J. S. Xu, Y. Kedem, C. F. Li, and G. C. Guo, Observing momentum disturbance in double-slit "which-way" measurements, Sci. Adv. **5**, eaav9547 (2019).
[4] B. King, A. Di Piazza, and C. H. Keitel, A matterless double slit, Nat. Photonics **4**, 92 (2010).
[5] M. Waitz *et al.*, Two-Particle Interference of Electron Pairs on a Molecular Level, Phys. Rev. Lett. **117**, 083002 (2016).
[6] M. Lyubomirskiy, I. Snigireva, and A. Snigirev, Lens coupled tunable Young's double pinhole system for hard X-ray spatial coherence characterization, Opt. Express **24**, 13679 (2016).
[7] R. K. Kushawaha, M. Patanen, R. Guillemin, L. Journel, C. Miron, M. Simon, M. N. Piancastelli, C. Skates, and P. Decleva, From double-slit interference to structural information in simple hydrocarbons, Proc. Natl. Acad. Sci. U.S.A. **110**, 15201 (2013).
[8] S. E. Canton, E. Plésiat, J. D. Bozek, B. S. Rude, P. Decleva, and F. Martín, Direct observation of Young's double-slit interferences in vibrationally resolved photoionization of diatomic molecules, Proc. Natl. Acad. Sci. U.S.A. **108**, 7302 (2011).
[9] H. D. Cohen and U. Fano, Interference in the photoionization of molecules, Phys. Rev. **150**, 30 (1966).
[10] D. Akoury, K. Kreidi, T. Jahnke *et al.*, The simplest double slit: Interference and entanglement in double photoionization of $H_2$, Science **318**, 949 (2007).
[11] J. Fernández, O. Fojón, A. Palacios, and F. Martín, Interferences from Fast Electron Emission in Molecular Photoionization, Phys. Rev. Lett. **98**, 043005 (2007).
[12] D. Rolles, M. Braune, S. Cvejanović *et al.*, Isotope-induced partial localization of core electrons in the homonuclear molecule $N_2$, Nature (London) **437**, 711 (2005).
[13] M. Kunitski, N. Eicke, P. Huber, J. Köhler *et al.*, Double-slit photoelectron interference in strong-field ionization of the neon dimer, Nat. Commun. **10**, 1 (2019).
[14] F. Lindner, M. G. Schätzel, H. Walther, A. Baltuška, E. Goulielmakis, F. Krausz, D. B. Milošević, D. Bauer, W. Becker, and G. G. Paulus, Attosecond Double-Slit Experiment, Phys. Rev. Lett. **95**, 040401 (2005).
[15] M. Richter, M. Kunitski, M. Schöffler, T. Jahnke, L. P. H. Schmidt, M. Li, Y. Q. Liu, and R. Dörner, Streaking Temporal Double-Slit Interference by an Orthogonal Two-Color Laser Field, Phys. Rev. Lett. **114**, 143001 (2015).
[16] X. Xie, T. Wang, S. Yu, X. Y. Lai, S. Roither, D. Kartashov, A. Baltuška, X. J. Liu, A. Staudte, and M. Kitzler, Disentangling Intracycle Interferences in Photoelectron Momentum Distributions Using Orthogonal Two-Color Laser Fields, Phys. Rev. Lett. **119**, 243201 (2017).
[17] J. Pursehouse, A. J. Murray, J. Wätze, and J. Berakdar, Dynamic Double-Slit Experiment in a Single Atom, Phys. Rev. Lett. **122**, 053204 (2019).
[18] M. Gavrila, Atomic stabilization in superintense laser fields, J. Phys. B **35**, R147 (2002).
[19] A. M. Popov, O. V. Tikhonova, and E. A. Volkova, Strong-field atomic stabilization: Numerical simulation and analytical modelling, J. Phys. B **36**, R125 (2003).
[20] Q. Wei, P. Wang, S. Kais, and D. Herschbach, Pursuit of the Kramers-Henneberger atom, Chem. Phys. Lett. **683**, 240 (2017).
[21] W. C. Henneberger, Perturbation Method for Atoms in Intense Laser Fields, Phys. Rev. Lett. **21**, 838 (1968).
[22] K. C. Kulander, K. J. Schafer, and J. L. Krause, Dynamic Stabilization of Hydrogen in an Intense, High-Frequency, Pulsed Laser Field, Phys. Rev. Lett. **66**, 2601 (1991).

[23] K. Toyota, O. I. Tolstikhin, T. Morishita, and S. Watanabe, Slow Electrons Generated by Intense High-Frequency Laser Pulses, Phys. Rev. Lett. **103**, 153003 (2009).

[24] Q. C. Ning, U. Saalmann, and J. M. Rost, Electron Dynamics Driven by Light-Pulse Derivatives, Phys. Rev. Lett. **120**, 033203 (2018).

[25] P. V. Demekhin and L. S. Cederbaum, Dynamic Interference of Photoelectrons Produced by High-Frequency Laser Pulses, Phys. Rev. Lett. **108**, 253001 (2012).

[26] M. Baghery, U. Saalmann, and J. M. Rost, Essential Conditions for Dynamic Interference, Phys. Rev. Lett. **118**, 143202 (2017).

[27] W. C. Jiang and J. Burgdörfer, Dynamic interference as signature of atomic stabilization, Opt. Express **26**, 19921 (2018).

[28] R. Moessner and S. L. Sondhi, Equilibration and order in quantum Floquet matter, Nat. Phys. **13**, 424 (2017).

[29] T. Nubbemeyer, K. Gorling, A. Saenz, U. Eichmann, and W. Sandner, Strong-Field Tunneling Without Ionization, Phys. Rev. Lett. **101**, 233001 (2008).

[30] U. Eichmann, T. Nubbemeyer, H. Rottke, and W. Sandner, Acceleration of neutral atoms in strong short-pulse laser fields, Nature (London) **461**, 1261 (2009).

[31] M. Richter, S. Patchkovskii, F. Morales, O. Smirnova, and M. Ivanov, The role of the Kramers-Henneberger atom in the higher-order Kerr effect, New J. Phys. **15**, 083012 (2013).

[32] M. Matthews, F. Morales, A. Patas *et al.*, Amplification of intense light fields by nearly free electrons, Nat. Phys. **14**, 695 (2018).

[33] M. P. De Boer, J. H. Hoogenraad, R. B. Vrijen, and H. G. Muller, Indications of High-Intensity Adiabatic Stabilization in Neon, Phys. Rev. Lett. **71**, 3263 (1993).

[34] M. V. Fedorov and A. M. Movsesyan, Field-induced effects of narrowing of photoelectron spectra and stabilisation of Rydberg atoms, J. Phys. B **21**, L155 (1988).

[35] A. M. Popov, O. V. Tikhonova, and E. A. Volkova, Applicability of the Kramers-Henneberger approximation in the theory of strong-field ionization, J. Phys. B **32**, 3331 (1999).

[36] F. Morales, M. Richter, S. Patchkovskii, and O. Smirnova, Imaging the Kramers-Henneberger atom, Proc. Natl. Acad. Sci. U.S.A. **108**, 16906 (2011).

[37] M. Pont, N. R. Walet, M. Gavrila, and C. W. McCurdy, Dichotomy of the Hydrogen Atom in Superintense, High-Frequency Laser Fields, Phys. Rev. Lett. **61**, 939 (1988).

[38] J. H. Eberly and K. C. Kulander, Atomic stabilization by super-intense lasers, Science **262**, 1229 (1993).

[39] R. Kosloff and H. Tal-Ezer, A direct relaxation method for calculating eigenfunctions and eigenvalues of the Schrödinger equation on a grid, Chem. Phys. Lett. **127**, 223 (1986).

[40] See Supplemental Material at http://link.aps.org/supplemental/10.1103/PhysRevLett.124.163201 for details, which includes Ref. [41].

[41] P. L. He and F. He, Ionization of $H_2^+$ in XUV pulses, Phys. Scr. **90**, 045402 (2015).

[42] J. Grochmalicki, M. Lewenstein, and K. Rzaewski, Stabilization of Atoms in Superintense Laser Fields: Is it Real?, Phys. Rev. Lett. **66**, 1038 (1991).

[43] M. Pont, N. R. Walet, and M. Gavrila, Radiative distortion of the hydrogen atom in superintense, high-frequency fields of linear polarization, Phys. Rev. A **41**, 477 (1990).

[44] A. S. Alnaser, X. M. Tong, T. Osipov, S. Voss, C. M. Maharjan, B. Shan, Z. Chang, and C. L. Cocke, Laser-peak-intensity calibration using recoil-ion momentum imaging, Phys. Rev. A **70**, 023413 (2004).

[45] M. Odenweller, N. Takemoto, A. Vredenborg, K. Cole, K. Pahl, J. Titze, L. P. H. Schmidt, T. Jahnke, R. Dörner, and A. Becker, Strong Field Electron Emission from Fixed in Space $H_2^+$ Ions, Phys. Rev. Lett. **107**, 143004 (2011).

[46] P. L. He, N. Takemoto, and F. He, Photoelectron momentum distributions of atomic and molecular systems in strong circularly or elliptically polarized laser fields, Phys. Rev. A **91**, 063413 (2015).

[47] T. Seideman, M. Y. Ivanov, and P. B. Corkum, Role of Electron Localization in Intense-Field Molecular Ionization, Phys. Rev. Lett. **75**, 2819 (1995).

[48] T. Zuo and A. D. Bandrauk, Charge-resonance-enhanced ionization of diatomic molecular ions by intense lasers, Phys. Rev. A **52**, R2511 (1995).

[49] J. Moody, A. Shapere, and F. Wilczek, Realizations of Magnetic-Monopole Gauge Fields: Diatoms and Spin Precession, Phys. Rev. Lett. **56**, 893 (1986).

[50] M. V. Berry, Quantal phase factors accompanying adiabatic changes, Proc. R. Soc. A **392**, 45 (1984).

[51] F. Wilczek and A. Zee, Appearance of Gauge Structure in Simple Dynamical Systems, Phys. Rev. Lett. **52**, 2111 (1984).

[52] Q. Ji, S. Pan, P. He, J. Wang, P. Lu, H. Li, X. Gong, K. Lin, W. Zhang, J. Ma, H. Li, C. Duan, P. Liu, Y. Bai, R. Li, F. He, and J. Wu, Timing Dissociative Ionization of $H_2$ Using a Polarization-Skewed Femtosecond Laser Pulse, Phys. Rev. Lett. **123**, 233202 (2019).

[53] I. Barth and O. Smirnova, Spin-polarized electrons produced by strong-field ionization, Phys. Rev. A **88**, 013401 (2013).

[54] A. Hartung, F. Morales, M. Kunitski *et al.*, Electron spin polarization in strong-field ionization of xenon atoms, Nat. Phys. **10**, 526 (2016).

[55] K. L. Liu, K. Renziehausen, and I. Barth, Producing spin-polarized photoelectrons by using the momentum gate in strong-field ionization experiments, Phys. Rev. A **95**, 063410 (2017).

[56] M. M. Liu, Y. Shao, M. Han, P. Ge, Y. K. Deng, C. Y. Wu, Q. H. Gong, and Y. Q. Liu, Energy- and Momentum-Resolved Photoelectron Spin Polarization in Multiphoton Ionization of Xe by Circularly Polarized Fields, Phys. Rev. Lett. **120**, 043201 (2018).

[57] D. Trabert, A. Hartung, S. Eckart, F. Trinter, A. Kalinin, M. Schöffler, L. P. H. Schmidt, T. Jahnke, M. Kunitski, and R. Dörner, Spin and Angular Momentum in Strong-Field Ionization, Phys. Rev. Lett. **120**, 043202 (2018).

[58] P. L. He, D. Lao, and F. He, Strong Field Theories Beyond Dipole Approximations in Nonrelativistic Regimes, Phys. Rev. Lett. **118**, 163203 (2017).

[59] A. A. Sorokin, S. V. Bobashev, T. Feigl, K. Tiedtke, H. Wabnitz, and M. Richter, Photoelectric Effect at Ultrahigh Intensities, Phys. Rev. Lett. **99**, 213002 (2007).